X-Ray Second Harmonic Generation

S. Shwartz,[1,2,*] M. Fuchs,[3,4] J. B. Hastings,[5] Y. Inubushi,[6] T. Ishikawa,[6] T. Katayama,[7] D. A. Reis,[3,8] T. Sato,[6] K. Tono,[7] M. Yabashi,[6] S. Yudovich,[1] and S. E. Harris[2]

[1]*Physics Department and Institute of Nanotechnology, Bar Ilan University, Ramat Gan 52900, Israel*
[2]*Edward L. Ginzton Laboratory, Stanford University, Stanford, California 94305, USA*
[3]*PULSE Institute, SLAC National Accelerator Laboratory, Menlo Park, California 94025, USA*
[4]*Department of Physics and Astronomy, University of Nebraska, Lincoln, Nebraska 68588, USA*
[5]*The Linac Coherent Light Source, SLAC National Accelerator Laboratory, Menlo Park, California 94025, USA*
[6]*RIKEN SPring-8 Center, Kouto 1-1-1 Sayo, Hyogo 679-5148, Japan*
[7]*Japan Synchrotron Radiation Research Institute, JASRI, Kouto 1-1-1 Sayo, Hyogo 679-5148, Japan*
[8]*Department of Applied Physics, Stanford University, Stanford, California 94305, USA*

(Received 1 November 2013; published 22 April 2014)

We report clear experimental evidence for second harmonic generation at hard x-ray wavelengths. Using a 1.7 Å pumping beam generated by a free electron laser, we observe second harmonic generation in diamond. The generated second harmonic is of order 10 times the background radiation, scales quadratically with pump pulse energy, and is generated over a narrow phase-matching condition. Of importance for future experiments, our results indicate that it is possible to observe nonlinear x-ray processes in crystals at pump intensities exceeding 10^{16} W/cm^2.

DOI: 10.1103/PhysRevLett.112.163901 PACS numbers: 42.65.Ky, 78.70.Ck

It is now 40 years since Freund [1] and Eisenberger [2] and colleagues described a theory for the nature of a solid-state dense plasma nonlinearity that is operative at x-ray wavelengths. The main assumption of this model is that since all pertinent photon energies are much higher than the binding energies of the electrons in light elements, the electrons can be treated as free particles, and the dominant nonlinearity is a plasmalike nonlinearity. This nonlinearity is very different from conventional nonlinearities in the visible regime. It is nonlocal, second order, and may be observed in centrosymmetric materials, but requires a nonuniform electron density. Unlike visible light, which interacts only with valence electrons, x-ray radiation interacts with both the valence and core electrons. It is well known that if the interacting photon energies are all above the electron binding energies, as in the case of the x rays, the magnitudes of nonlinearities are very small. Consequently, previous to the work reported here, hard x-ray nonlinearities have only been observed in parametric down-conversion [2–9]. The key factor for those experiments is the large number of vacuum fluctuation modes at x-ray wavelengths. Thus, although the parametric gain is very small, coincidences of the generated signal and idler photons can be measured even when the pump source is an x-ray tube [2].

X-ray free electron lasers (XFELs) are revolutionizing the study of atomic-scale structure and dynamics [10–17]. For applications including coherent imaging, focused intensities in excess of 10^{19} W/cm^2 are often used [18]. At these intensities, the x-ray matter interaction is characterized by multiple sequential ionization, raising questions for interpretation of experiments [10–17,19]. Recently, Glover and colleagues have demonstrated the nonlinear wave mixing of x-ray and near-infrared beams [20]. However, the efficiency in those experiments depends on the intensity of the infrared laser and not on the intensity of the x-ray laser. On the other hand, the high peak power of the XFEL is critical for the observation of most x-ray nonlinear effects. For example, the theory based on the plasma nonlinearity predicts that the observation of x-ray second harmonic generation (SHG) requires pump intensities exceeding 10^{15} W/cm^2. These intensities are orders of magnitude larger than the damage threshold in the visible regime, and the corresponding electric field strengths are nearly the atomic field.

In this Letter, we report an experimental investigation of one of the most fundamental nonlinear processes at x-ray wavelengths. We measure the generation of the second harmonic of a 1.7 Å (7.3 keV) pumping beam from the SACLA XFEL. Working at an average intensity of $\sim 10^{16}$ W/cm^2, and using a diamond crystal, we observe a SHG signal at a rate of about 1 photon for every 150 x-ray laser shots. This signal is about 10 times higher than the background. The second harmonic beam is generated in a narrow angular range of ~0.2 mrad full width at half maximum (FWHM) and scales quadratically with pump-pulse energy.

Similar to SHG in the visible regime, the efficiency of x-ray SHG depends strongly on phase matching. Unlike visible SHG, at hard x-ray wavelengths, phase matching cannot be achieved in the forward direction. However, it can be achieved in other directions by using the periodic nature of the electron density in crystals. Phase matching occurs when $2\vec{k}_\omega + \vec{G} = \vec{k}_{2\omega}$, where $\vec{k}_\omega$, $\vec{k}_{2\omega}$ are the internal

wave vectors of the pump and second harmonic beams, respectively, and $\vec{G}$ is a reciprocal lattice vector [21]. Because of the finite dispersion, the angles (θ_ω and $\theta_{2\omega}$) between these beams and the atomic planes differ slightly from the linear Bragg diffraction condition for the second harmonic.

The experiment is performed at BL3 SPring-8 Angstrom Compact XFEL (SACLA) in Hyogo, Japan [22]. The experimental setup is shown in Fig. 1. We design the experiment to suppress the second harmonic in the pump beam generated in the XFEL [23–25], as well as parasitic scatter of the pump. A Si (111) double-crystal monochromator is used to select a narrow (1 eV) bandwidth pump beam centered at 7.3 keV. The monochromator setting corresponds to the Si (222) Bragg diffraction condition for the second harmonic, which is forbidden. This results in more than 4 orders of magnitude suppression of the undulator second harmonic. After monochromatization the beam is focused by a pair of grazing incidence mirrors in the Kirkpatrick-Baez (KB) geometry [26] to an approximately 1.5 μm FWHM spot at the sample (the corresponding Rayleigh range is 30 mm and the divergence is 41 μrad for a lowest order Gaussian beam). A set of thin Al prefilters are inserted before the KB mirrors to attenuate the fundamental and have negligible effect on the transmission of the residual harmonics. The pulse energy before the prefilters is measured on a shot-by-shot basis. The sample is a 0.48 mm thick (111) cut diamond single crystal and is placed in the focus of the x-ray beam. We choose to phase match with the C(220) reciprocal lattice vector. This corresponds to the C(110) reflection for the fundamental which is strictly forbidden in the face-centered cubic structure; thus, elastic scattering of the pump fundamental is highly suppressed. Scattered photons near $\theta_{2\omega}$ are detected by a YAP:Ce scintillation detector with energy resolution of ~30%. Note that the detector cannot distinguish a single second harmonic photon from two fundamental photons on any given pulse. Moreover, the probability of measuring two photons per pulse scales quadratically with incident pulse energy at low count rates. We use slits between the sample and the detector combined with a thick Al postfilter to reduce background photons at the fundamental wavelength [27]. We empirically set the filter thickness to reduce the Poisson statistics for two fundamental photons to well below the measured second harmonic count rate.

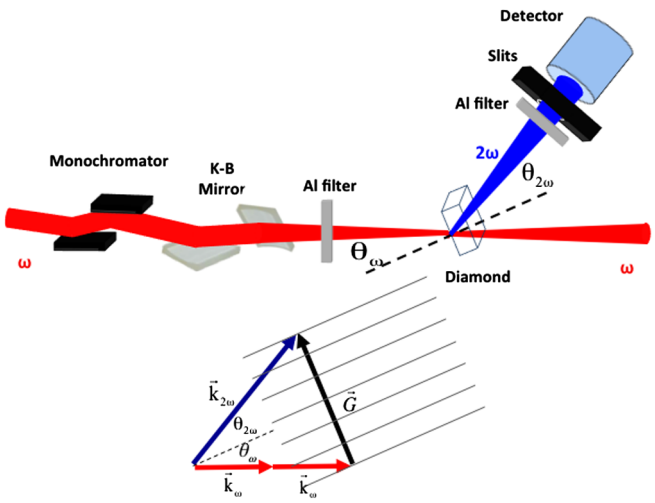

FIG. 1 (color online). Schematic of the SHG experimental setup. X-ray pulses are incident to a silicon (111) channel cut monochromator. The monochromator selects a 7.3 keV pump beam with 1 eV bandwidth while rejecting a substantial fraction of the second harmonic contamination. A pair of Kirkpatrick Baez mirrors focuses the beam to about 1.5 μm while reducing the third harmonic contamination. The nonlinear medium is a (111) cut diamond crystal placed in the focus and set for phase matching as indicated in the phase matching diagram (bottom). The phase matching is achieved by using the (220) atomic planes, $\vec{k}_\omega$ and $\vec{k}_{2\omega}$ are the wave vectors of the pump and the generated second harmonic, respectively. $\vec{G}$ is the reciprocal lattice vector orthogonal to the (220) atomic planes. We control the intensity of the pump by using a set of Al filters before the sample. The second harmonic is detected using a scintillator crystal and photomultiplier tube with additional filters used to reduce the probability of detecting multiple 7.3 keV photons per pulse.

Since the intensities in our experiment exceed 10^{16} W/cm^2, we check for damage by measuring the elastic scattering of the C(220) peak for 7.3 keV at reduced intensity (19%) and comparing it with maximum pulse energy after an exposure of about 10 min corresponding to approximately 6000 shots. We observe no significant changes in the peak reflectivity or in the width of the rocking curve (approximately 280 μrad) between the low and high intensity before and after irradiation. This width is larger than the width predicted by the numerical simulation of the slowly varying envelope equations (120 μrad).

A histogram of detector counts as a function of photon energy is shown in Fig. 2 at full intensity (no prefilter) and at the peak of the phase matching condition for 24000 shots. The energy bin width is 1.39 keV. The data of Fig. 2(a) consist of two peaks corresponding to photon energies near the fundamental and second harmonic. We define upper- and lower-level thresholds for registering a count as a second harmonic photon as 10.2–19 keV (+/− 30% of 14.6 keV) and 5.1–9.5 keV for the fundamental. Within these limits, we measure 153 second harmonic photons ($\sim 0.0064 \pm 0.0005$/pulse), compared to 35 fundamental photons (0.0015 ± 0.0002/pulse). The quoted uncertainties assume shot-noise limited statistics. The few counts that register more than the energy of a second harmonic could be due to third harmonic contamination from the FEL [28]. The relatively small probability of detecting a single fundamental photon per shot and the predominance of counts at the second harmonic energy indicates that the background due to either pulse pile-up or contamination from the finite resolution of the detector is negligible.

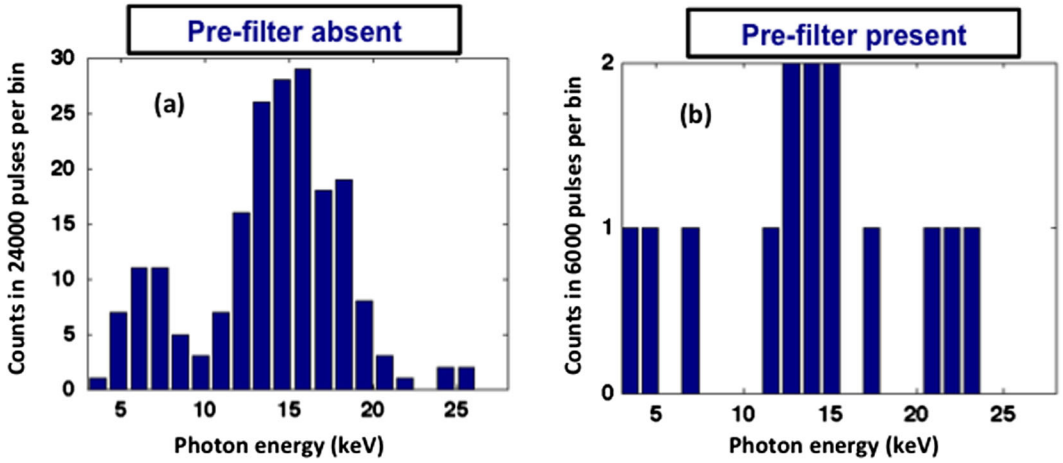

FIG. 2 (color online). Photon-energy histograms of the measured signal at the peak of the phase-matching condition. The pump-photon energy is 7.3 keV and the SHG photon energy is 14.6 keV. The energy resolution of the detector is ~30%. The data in part (a) are taken with no attenuation. The data in part (b) are taken with a 0.025 mm Al filter before the diamond crystal (the transmission through the filter is 0.43 and 0.9 at 7.3 and 14.6 keV, respectively).

Next we determine whether the measured second harmonic photons originate from the x-ray SHG in the crystal or from the residual second harmonic photons generated from the XFEL. A distinguishing characteristic of the SHG is the nonlinear dependence on the incident intensity. To differentiate the two possibilities, we insert a 0.025 mm Al prefilter before the diamond crystal to preferentially attenuate the fundamental. The absorption coefficients for Al at the fundamental and second harmonic are 168 and 21.8 cm^{-1} [29] corresponding to transmission through the prefilter of 0.43 and 0.9, respectively. The resulting histogram is plotted in Fig. 2(b). In this case we count only 7 second harmonic photons in 6000 pulses (~0.0015 ± 0.0005/pulse). This count rate is approximately 4 times smaller than the count rate with no prefilter. Since the transmission of the undulator second harmonic through the prefilter is approximately 90%, the reduction of the measured second harmonic signal by a factor of 4 indicates that most of the second harmonic signal we measure with no prefilter is generated in the crystal.

We repeat the measurement for several different prefilter settings (no filter, 0.025, 0.1, and 0.2 mm Al). Figure 3(a) shows the second harmonic count rate as a function of the average of the pump pulse energy when the crystal is detuned by -57 μrad from the peak of the phase matching condition. Figure 3(b) shows the rocking curve of the SHG process, namely, the second harmonic count rate as a function of the angular deviation of the crystal from the

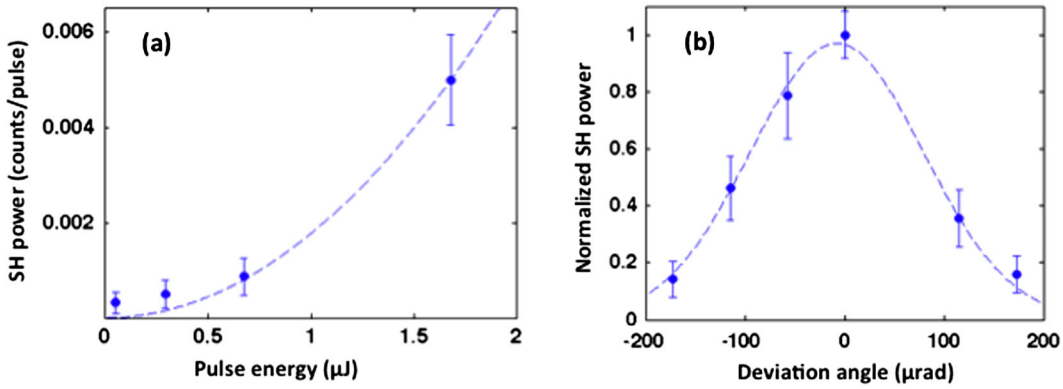

FIG. 3 (color online). Scaling of second harmonic rate with average pump pulse energy and angular deviation. (a) Detected second harmonic signal as a function of input pulse energy and measured at angular deviation of -57 μrad from the SHG phase-matching angle. The pulse energy is varied by inserting thin Al filters before the diamond crystal. Each of the measured data points represents an average over 6000 pulses. The dashed blue curve is calculated from the solutions Eq. (2) with a Gaussian chirp model and scaled vertically by a factor of 1.48. (b) Normalized second harmonic signal as a function of the angular deviation of the diamond crystal from the phase matching angle. The data in part (b) are obtained with no attenuation before the diamond crystal. The dashed curve is a Gaussian fit to the experimental data. The FWHM of the rocking curve is 180 μrad. The peak point represents the average signal measured over 2400 pulses. The other points represent the average signal measured over 6000 pulses. The vertical error bars indicate the counting statistics.

phase matching angle. Consistent with the data on the peak of the phase matching condition, the second harmonic signal at -57 μrad [Fig 3(a)] upon inserting the 0.025 mm prefilter is reduced to $18 \pm 8\%$ of the value without the filter. It is clear from Fig. 3(a) that the count rates at the two lowest pulse energies are equal within the statistical uncertainty. We use this to estimate the residual second harmonic assuming that it dominates the measurement at the lowest pulse-energy. After correcting for the filter transmission, we find that the residual harmonic corresponds to 0.0054 ± 0.0030 counts/pulse. Thus, from Fig. 3 we conclude that the SHG from the crystal is about a factor of 10 higher than the background at the highest intensity. We plot a Gaussian fit and find the FWHM of the rocking curve is approximately 180 μrad.

The data shown in Figs. 2 and 3 are the average values over a large number of pulses. We now use the large pulse-to-pulse fluctuations of the FEL pulse energy to investigate the dependence of the second harmonic count rate on the pulse energy. The measured pulse-energy histogram of the FEL beam is shown in the inset of Fig. 4. We expect that the SHG signal will scale quadratically with pulse energy assuming that the second harmonic contamination is linear in the pulse energy. We start by building histograms of the number of pulses at a given pump pulse energy. We scan through the recorded data and count the number of second harmonic photons measured within each pump pulse-energy bin. We iteratively vary the bin widths, and recount the second harmonic photons, until the number of second harmonic counts in each bin is between 24 and 26. We calculate the count rate by dividing the number of second harmonic counts in each bin by the number of pulses with pulse-energy within the bin. The resultant second harmonic count rate as a function of the pulse-energy of the pump is shown in Fig. 4. The blue circles show experimental data, and the dashed curve is the result of a polynomial fit. We find that the dependence of the measured signal on the pulses-energy of the pump can be expressed as $N_{\mathrm{SHG}} = 0.0014 \pm 0.0002U^2 + 0.0013 \pm 0.0008U$. Here, N_{SHG} is the number of second harmonic counts per pulse, and U is the pulse energy of the pump in μJ. At the lowest pulse energies the dependence is primarily linear, while at the higher pulse energies ($U > 1$) the dependence is primarily quadratic. We conclude that SHG dominates at pulse energies larger than 1 μJ. This is consistent with the results of Fig. 3. We attribute the linear term with residual undulator second harmonic contamination that scales with the fundamental pulse energy.

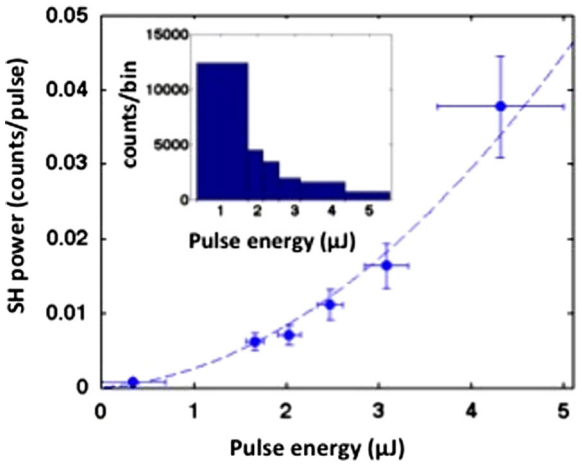

FIG. 4 (color online). Detected second harmonic rate as a function of the pulse energy of the pump at the phase matching condition. The pulse-energy dependence is obtained from the pulse-energy fluctuations of the XFEL beam. The dashed line is the polynomial fit to the experimental data as described in the text. The vertical error bars indicate the counting statistics. The horizontal error bars are the standard deviation of the pulse energy within a bin. The inset shows the histogram of the pulse energy of the XFEL beam.

We compare our experimental results with the theory of x-ray SHG. In the cold plasma approximation, the nonlinearity is described by the nonlinear current density. We assume phase matching with a single reciprocal lattice vector $\vec{G}$, and the envelope for the nonlinear current density at the second harmonic is given by [21]

$$J_{2\omega}(\vec{r}, t) = -\frac{q^2 \rho_G G \cos(\theta_B)}{8m^2\omega^3} \phi(\theta_B)[E_\omega(\vec{r}, t)]^2. \quad (1)$$

Here, q and m are the electron charge and mass, and ρ_G is the Fourier component of the electron density corresponding to the reciprocal lattice vector $\vec{G}$. θ_B is the Bragg angle, and $\phi(\theta_B) = [1 - 4\cos(2\theta_B)]$ for a pump polarized in the scattering plane [21]. $E_\omega(\vec{r}, t)$ is the envelope of the electric field of the pumping beam.

The second harmonic beam is emitted at an angle of $\theta_\omega + \theta_{2\omega}$ (about 39°) with respect to the fundamental driving beam. This leads to a finite distance over which both beams overlap. For transparent crystals that are thicker than the interaction length, the SHG efficiency is expected to grow as the propagation length, and not as its square, as in conventional nonlinear optics [30]. For our experimental conditions, the interaction length is about 1 μm assuming a 1.5 μm beam spot and a 20 fs duration pulse [31].

The slowly varying envelope equation for the second harmonic field is

$$\cos(\theta_{2\omega})\frac{\partial E_{2\omega}}{\partial z} + \sin(\theta_{2\omega})\frac{\partial E_{2\omega}}{\partial x} + \frac{1}{v_{2\omega}}\frac{\partial E_{2\omega}}{\partial t} = -\frac{\eta}{2} J_{2\omega}. \quad (2)$$

Here $v_{2\omega}$ is the group velocity of the SHG field. We solve the equation for a 1 eV bandwidth.

We define the SHG efficiency as the number of second harmonic photons per pump photon. We find that the maximum measured efficiency is $5.8 \pm 1.1 \times 10^{-11}$ for a pump pulse energy of 4.3 μJ (3.7×10^9 photons per pulse) after correction for the finite absorption of the Al postfilter. The result compares well with the calculated efficiency of

5×10^{-11} assuming a Gaussian chirp model. However, we find that the calculated rocking curve width is 50 μrad FWHM while the measured width is about 180 μrad. To test the influence of the spiky nature of the XFEL pulses on the efficiency, we obtain the right-hand side of Eq. (2) by constructing a randomly phased train of transform limited pulses with a pulse duration, and a time difference between pulses, both equal to 1.5 fs. We multiply the train by a Gaussian window of 20 fs FWHM. We then fast Fourier transform and solve numerically in the frequency domain. This result is averaged over 200 runs each with different random phases between pulses. This model predicts an efficiency of 6.75×10^{-11} and a width of 50 μrad FWHM. This suggests that the spiky nature of the FEL pulses could affect the efficiency, but the difference is small with respect to other uncertainties such as the actual pulse duration. Finally, we calculate the efficiency for a transform-limited source with a bandwidth of 1 eV. This model predicts an efficiency of 5.4×10^{-10} and the rocking curve width is 50 μrad FWHM.

In summary, we report clear evidence for SHG at hard x-ray wavelengths. The generated second harmonic count rate scales as the square of the pump pulse energy, and its magnitude peaks at the phase matching angle. The largest observed SHG efficiency is 5.8×10^{-11} with a count rate that is more than 10 times above the background. The second harmonic is generated with an average fundamental x-ray intensity of on the order of 10^{16} W/cm^2 , corresponding to an electric field at the peak of the pulse of about 2.5×10^9 V/cm. This corresponds very nearly to the atomic unit of field strength. The results described in this Letter advance our understanding of x-ray matter interactions at high intensity and form the basis for more general experiments on x-ray nonlinear processes. For example, future experiments might explore x-ray phase conjugation, squeezing, and the generation of polarization entangled x-ray photons.

This work was supported by the U.S. Air Force Office of Scientific Research and the U.S. Army Research Office and by the Israel Science Foundation. D. A. R. acknowledges support by the AMOS program within the Chemical Sciences division of the Office of Basic Energy Sciences, Office of Science, U.S. Department of Energy. M. F. gratefully acknowledges support by the Volkswagen Foundation. The XFEL experiments were performed at the BL 3 of SACLA with the approval of the Japan Synchrotron Radiation Research Institute (JASRI) (Proposal No. 2012A8033).

*Sharon.shwartz@biu.ac.il

[1] I. Freund and B. F. Levine, Phys. Rev. Lett. **23**, 854 (1969).
[2] P. M. Eisenberger and S. L. McCall, Phys. Rev. Lett. **26**, 684 (1971).
[3] B. W. Adams, *Nonlinear Optics, Quantum Optics, and Ultrafast Phenomena with X-Rays* (Kluwer Academic, Norwell, MA, 2008).
[4] B. Adams, Y. Nishino, D. V. Novikov, G. Materlik, and D. M. Mills, Nucl. Instrum. Methods Phys. Res., Sect. A **467–468**, 1019 (2001).
[5] B. Adams, P. Fernandez, W.-K. Lee, G. Materlik, D. M. Mills, and D. V. Novikov, J. Synchrotron Radiat. **7**, 81 (2000).
[6] K. Tamasaku and T. Ishikawa, Phys. Rev. Lett. **98**, 244801 (2007).
[7] K. Tamasaku, K. Sawada, and T. Ishikawa, Phys. Rev. Lett. **103**, 254801 (2009).
[8] K. Tamasaku, K. Sawada, E. Nishibori, and T. Ishikawa, Nat. Phys. **7**, 705 (2011).
[9] S. Shwartz, R. N. Coffee, J. M. Feldkamp, Y. Feng, J. B. Hastings, G. Y. Yin, and S. E. Harris, Phys. Rev. Lett. **109**, 013602 (2012).
[10] L. Young *et al.*, Nature (London) **466**, 56 (2010).
[11] L. Fang *et al.*, Phys. Rev. Lett. **105**, 083005 (2010).
[12] B. Rudek *et al.*, Nat. Photonics, **6**, 858 (2012).
[13] P. Salen *et al.*, Phys. Rev. Lett. **108**, 153003 (2012).
[14] S. Schorb *et al.*, Phys. Rev. Lett. **108**, 233401 (2012).
[15] T. Gorkhover *et al.*, Phys. Rev. Lett. **108**, 245005 (2012).
[16] C. Bostedt *et al.*, J. Phys. B **46** 164003 (2013).
[17] M. M. Seibert *et al.*, Nature (London) **470**, 78 (2011).
[18] H. N. Chapman *et al.*, Nature (London) **470**, 73 (2011).
[19] G. Doumy *et al.*, Phys. Rev. Lett. **106**, 083002 (2011).
[20] T. E. Glover *et al.*, Nature (London) **488**, 603 (2012).
[21] A. Nazarkin, S. Podorov, I. Uschmann, E. Forster, and R. Sauerbrey, Phys. Rev. A **67**, 041804(R) (2003).
[22] T. Ishikawa *et al.*, Nat. Photonics **6**, 540 (2012).
[23] G. Geloni, E. Saldin, E. Schneidmiller, and M. Yurkov, Opt. Commun. **271**, 207 (2007).
[24] H. P. Freund, S. G. Biedron, and S. V. Milton, IEEE J. Quantum Electron. **36**, 275 (2000).
[25] D. Ratner *et al.*, Phys. Rev. ST Accel. Beams **14**, 060701 (2011).
[26] H. Yumoto *et al.*, Nat. Photonics **7**, 43 (2013).
[27] From the thickness of the Al postfilter and the tabulated absorption coefficients [29], we estimate that the transmission of the fundamental wavelength is reduced by a factor of about 10^6 while the SHG beam is reduced by a factor of about 7.
[28] Note that a fraction of the 3rd harmonic of the FEL is selected by the Si monochromator but is partially rejected by the focusing mirrors. We estimate that the 3rd harmonic contamination before the diamond crystal is smaller than 10^4 photons/pulse. The (330) reflection of the diamond crystal is strictly forbidden in the bulk, but has a residual intensity due to surface truncation effects. However, we find the contribution from the 3rd harmonic counts to be insignificant.
[29] B. L. Henke, E. M. Gullikson, and J. C. Davis, At. Data Nucl. Data Tables **54**, 181 (1993).
[30] R. W. Boyd, *Nonlinear Optics* (Elsevier Inc., Burlington, MA, 2008).
[31] Y. Inubushi *et al.*, Phys. Rev. Lett. **109**, 144801 (2012).